Journal of Materials Chemistry A

PAPER

View Article Online
View Journal | View Issue



Cite this: J. Mater. Chem. A, 2015, 3, 21070

Received 6th August 2015
Accepted 10th September 2015

DOI: 10.1039/c5ta06156c

www.rsc.org/MaterialsA

# Elastic perovskite solar cells†

Jue Deng, Longbin Qiu, Xin Lu, Zhibin Yang, Guozhen Guan, Zhitao Zhang and Huisheng Peng*

Perovskite solar cells have attracted increasing attention due to the possibility of flexible devices compared with silicon-based photovoltaic cells and high energy conversion efficiencies compared with organic photovoltaic cells. Although they have been widely explored in recent years, elastic perovskite solar cells, for the first time, have been realized here by designing a stretchable nanostructured fiber and spring-like modified Ti wire as two electrodes with perovskite materials coated on the modified Ti wire based on a solution process. The elastic perovskite solar cell appears in a fiber format and maintains stable energy conversion efficiencies under stretching.

## Introduction

Silicon-based solar cells have long been recognized for their high energy conversion efficiencies such as 20.4% for multicrystalline silicon but with a rigid structure and high cost, which have limited their large-scale applications.[1,2] In contrast, polymer solar cells are widely studied for their flexible structure and low cost but with low energy conversion efficiencies.[3,4] Recently, a new family of promising photovoltaic devices, *i.e.*, perovskite solar cells (PSCs), have been extensively investigated for their high energy conversion efficiencies that are comparable with those of their silicon-based counterparts and possibility for a flexible structure and low cost similar to polymer solar cells.[5–8] PSCs have thus boosted the application of solar cells in a wide variety of fields and may particularly open an avenue to many new applications such as microelectronic devices. During the past years, a lot of attention has been paid to enhance the energy conversion efficiency by incorporating new materials and designing novel structures.[9–12] Recently, increasing efforts have been made to fabricate flexible devices to more effectively utilize the above advantages for the fabrication of portable and wearable electronic devices.[13,14] To this end, PSCs should be more elastic to withstand the stress produced during stretching and bending. Otherwise, they will break and fail to work in a short period of operation. Although elastic PSCs are highly desired for practical applications, they have not been realized yet.

On the other hand, it is also necessary while remaining challenging to make PSCs lightweight and wearable in modern electronics.[15–17] For instance, electronic textiles are proposed to be critically important in some emerging technologies including sensing electronic skins and wearable microelectronic products. However, because metallic films and perovskite layers on the elastic substrate are easily fractured or buckled during stretching, the planar structure of available PSCs cannot satisfy the above application.[14,18,19]

Herein, an elastic PSC fiber is developed by using a stretchable aligned carbon nanotube (CNT) based conducting fiber and a spring-like modified Ti wire as two electrodes with perovskite materials deposited on the modified Ti wire through an easy solution process. This novel fiber-shaped PSC exhibits a stable photovoltaic performance under both stretching and bending. In addition, the all-solid-state structure enables it to be woven into various electronic textiles.

## Experimental section

### Preparation of working electrodes based on aligned $TiO_2$ nanotubes

A rigid steel wire with a diameter of 1.8 mm was fixed on two synchronous motors. A washed Ti wire (diameter of 250 μm and purity of 99.7%) was uniformly wrapped on and then removed from the steel wire to form a spring-like shape. An electrochemical anodisation method was applied to grow $TiO_2$ nanotubes on the surface of Ti wire at a voltage of 20 V (the voltage was increased to 20 V at a sweeping rate of 250 mV $s^{-1}$).[20,21] The electrolyte was composed of water and glycerol (v/v, 1/1) and 0.27 M $NH_4F$. The spring-like Ti wire and a Pt sheet were used as the anode and cathode, respectively. The resulting wires were washed with deionized water to remove the electrolyte, followed by heating to 500 °C in 30 min and kept in air for 1 h.

### Preparation of working electrodes based on aligned $TiO_2$ nanoparticles

A spring-like Ti wire was immersed in a diluted titanium diisopropoxide bis(acetylacetonate) solution and then dried at

*State Key Laboratory of Molecular Engineering of Polymers, Department of Macromolecular Science, Laboratory of Advanced Materials, Fudan University, Shanghai 200438, China. E-mail: penghs@fudan.edu.cn*

† Electronic supplementary information (ESI) available. See DOI: 10.1039/c5ta06156c

125 °C. The thickness was tunable by repeating the dip-coating process. The modified Ti wire was annealed at 500 °C for 15 min in air, followed by treating with a $TiCl_4$ aqueous solution (40 mM) at 70 °C for 30 min. The washed wires were annealed at 500 °C for 30 min to form an n-type compact $TiO_2$ layer. A commercial $TiO_2$ nanoparticle (diameter of 20 nm) paste (DHS-TPP3, Heptachroma) was diluted in ethanol (w/w, 1/3) and then dip-coated on the compact $TiO_2$ layer. The resulting wires were gradually heated to 500 °C and annealed for 30 min at the same temperature.

### Fabrication of elastic PSCs

The fabrication of the elastic PSC fiber is schematically shown in Fig. 1a. The synthesis of perovskite materials is described in the ESI.† The modified spring-like Ti wire was dipped into the perovskite precursor solution for 30 s, lifted up at a speed of ~1 mm $s^{-1}$ and then annealed for 5 min, followed by cooling down to room temperature. The above process was repeated twice and finally annealed at 100 °C for 2 h. The hole transport material solution containing 0.170 M 2,2′,7,7′-tetrakis(*N*,*N*-di-*p*-methoxyphenylamine)-9,9′-spirobifluorene (spiro-MeOTAD, Chemsky International Co., Ltd), 0.064 M bis(trifluoromethane) sulfonamide lithium salt (LiTFSI, 99.95%, Aladdin) and 0.198 M 4-tertbutylpyridine (TBP, 96%, Aladdin) in a solvent mixture of chlorobenzene (99.8%, Aldrich) and acetonitrile (99.8%, Aldrich) (v/v, 10/1) was dip-coated onto the perovskite layer for 30 s in air. An elastic fiber was fabricated by injecting a liquid silicone rubber precursor into a tube with an inner diameter of 1.8 mm and then heated at 80 °C for 1 h for curing. The elastic fiber was extracted from the tube and wrapped with an aligned CNT sheet to form an elastic conductive fiber. The elastic conductive fiber was inserted into the spring-like modified Ti wire in a stretched state, and then released to a natural state favouring a close contact with the modified Ti wire. Another aligned CNT sheet was wrapped on the outer surface to produce the elastic PSC fiber.

### Calculation of the energy conversion efficiency

A PSC fiber was illuminated from the top during the measurement. The effective area of the working electrode was calculated as the projected area that has been generally used and recognized for a one-dimensional solar cell.[19] Fig. S1† schematically illustrates the calculation process, and the blue section of the working electrode was calculated as the effective area. The working electrode exhibits a three-dimensional helical structure and can be mathematically expressed as $X = A\cos\frac{2\pi Y}{T}$ and $Z = A\sin\frac{2\pi Y}{T}$. Here the amplitude $A$ can be calculated to be 1.09 mm and $T$ represents the pitch distance that is a constant of 1.25 mm. The projection area of the working electrode in the $Y$–$Z$ plane is expressed as $Z = 1.09\sin\frac{\pi Y}{0.625}$. For the working electrode, the length of the three-dimensional spiral can be calculated by the equation $L = \int\sqrt{1+\left(\frac{dZ}{dY}\right)^2}dY$, so $L = \int\sqrt{1+\left(\frac{1.09\pi}{0.625}\right)^2\cos^2\left(\frac{\pi Y}{0.625}\right)}dY$. A cycle of the projection area includes the shaded part $L_1 = \int_0^{1.25}\sqrt{1+29.99\cos^2(5.03Y)}dY = 4.619$ mm. For the shaded part, $Y$ is calculated to be 0.209 mm at $Z$ of 0.91 mm according

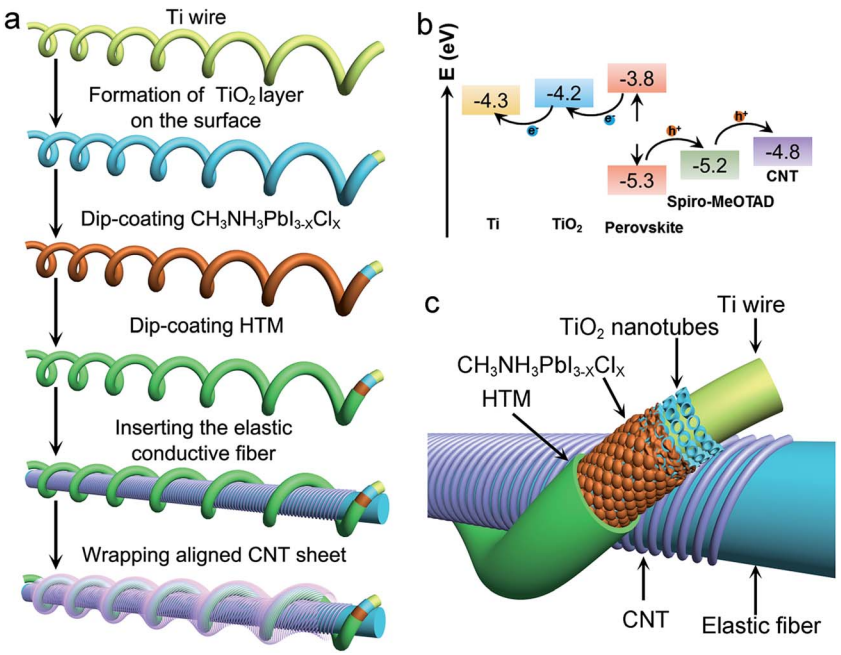


Fig. 1 Schematic illustration to the elastic PSC fiber. (a) Fabrication process. (b) Energy level diagram. (c) Structure.

to $Z = 1.09 \sin \frac{\pi Y}{0.625}$. Therefore, the arc length is obtained by $L_2 = \int_{-0.209}^{0.209} \sqrt{1 + 29.99 \cos^2(5.03Y)}\mathrm{d}Y = 1.938$ mm. Finally, the effective area ($S$) of the working electrode is evaluated by the equation $S = n \times D \times (L_1 - L_2) = n \times 0.263 \times 2.681 = 7.05 \times 10^{-3} \times$ n cm$^2$.

## Results and discussion

The working mechanism of the elastic PSC fiber is shown in Fig. 1b.[6,22] When $CH_3NH_3PbI_{3-x}Cl_x$ absorbs light, free carriers are created from incident photons, and electrons and holes are separated owing to the built-in electric field. Electrons and holes are transferred to the $TiO_2$ and the spiro-MeOTAD, and then collected by using a conductive Ti wire[23] and CNTs, respectively (Fig. 1c). Here Ti wire was used for the convenience to compare with the other fiber-shaped solar cells that used Ti wire electrodes. Due to over one-micrometer electron–hole diffusion lengths that are longer than the layer thickness, the charge collection is highly efficient offering a remarkable photovoltaic performance.[5,24,25]

The compositions and crystal lattice parameters of $CH_3NH_3PbI_{3-x}Cl_x$ are verified by X-ray diffraction (Fig. 2a). The formation of a uniform, continuous film on a curved surface is critical to the performance of the PSC fiber. Recently, some studies focused on controlling the preparation of uniform perovskite materials to avoid large crystal formation and low surface coverage.[26,27] Here, an additive, 1,8-diiodooctane (DIO), was introduced to enhance the crystallization of $CH_3NH_3PbI_{3-x}Cl_x$, which was verified by the increased peak intensity compared with the pristine perovskite material. In contrast, without the assistance of DIO, the crystallization process was fast and tended to produce large crystals, leading to a low surface coverage and high possibility for short-circuit in the device (Fig. S2, S3 and S4†). The enhancement from DIO was probably attributed to the chelation between $Pb^{2+}$ and DIO (Fig. 2b). DIO occupied two corners of the octahedron, preventing too rapid crystallization and production of large crystals by sharing the corner $I^-$ ion with the evaporation during annealing. The chelation mechanism was also verified by UV-vis spectra (Fig. 2c). The dilute precursor solution with introduction of low amounts of DIO resulted in a slight red shift compared with the dilute pristine precursor solution. In addition, the absorption peak was shifted from 264 to 269 nm (Fig. S5†), which agreed with the chelation between $Pb^{2+}$ and DIO.[28]

The highly aligned CNT sheet was dry-spun from a spinnable CNT array that was synthesized by chemical vapor deposition (Fig. S6†).[13,14,19,29,30] The high-resolution transmission electron microscopy image of CNTs (Fig. S7†) exhibited a multi-walled structure with an average diameter of ~10 nm. The thickness for a single layer of CNT sheet was typically ~20 nm, and many CNT sheets could be further stacked into thicker films along the CNT-aligned direction. The aligned CNT sheet may be stably attached on the surface of various substrates including the rubber fiber by the van der Waals force due to a high surface area.

Various $TiO_2$ nanomaterials have been widely studied for planar PSCs, and $TiO_2$ nanotubes and nanoparticles are here compared for the fiber-shaped PSC.[7,31–33] The $TiO_2$ nanotube array and nanoparticle layer were synthesized by electrochemical anodisation and dip-coating processes, respectively. The resulting $TiO_2$ demonstrated an anatase crystal structure after calcination at 500 °C (Fig. S8†). Fig. 3a and b show the comparison of their morphologies from a top view under a

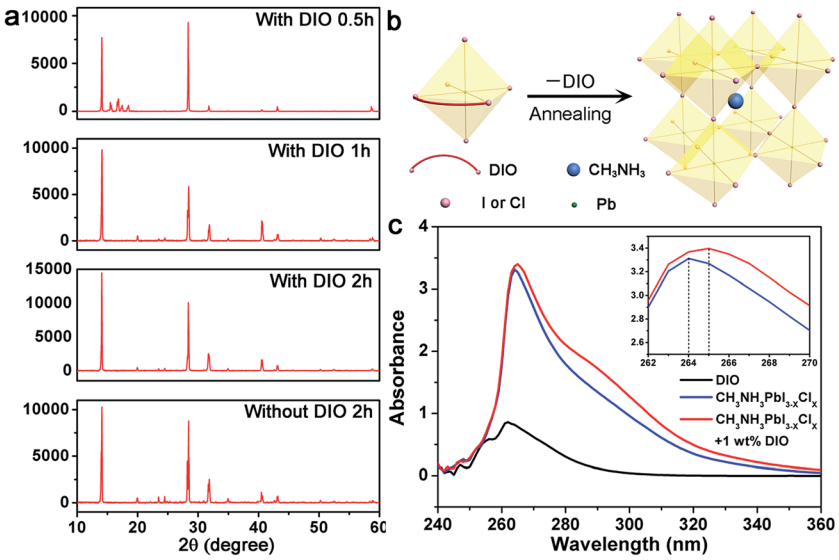


Fig. 2 (a) X-ray diffraction patterns of the $CH_3NH_3PbI_{3-x}Cl_x$ layer during evolution. (b) Schematic illustration to the formation of the perovskite material *via* the transient chelation of $Pb^{2+}$ with DIO. The octahedral molecule is composed of $Pb^{2+}$ transient chelated with DIO. During the annealing process, the DIO molecules are gradually evaporated, resulting in a uniform perovskite phase with corner-sharing octahedra. (c) UV-vis absorption spectra of DIO, $CH_3NH_3PbI_{3-x}Cl_x$ precursor solutions and a mixture of them.

 

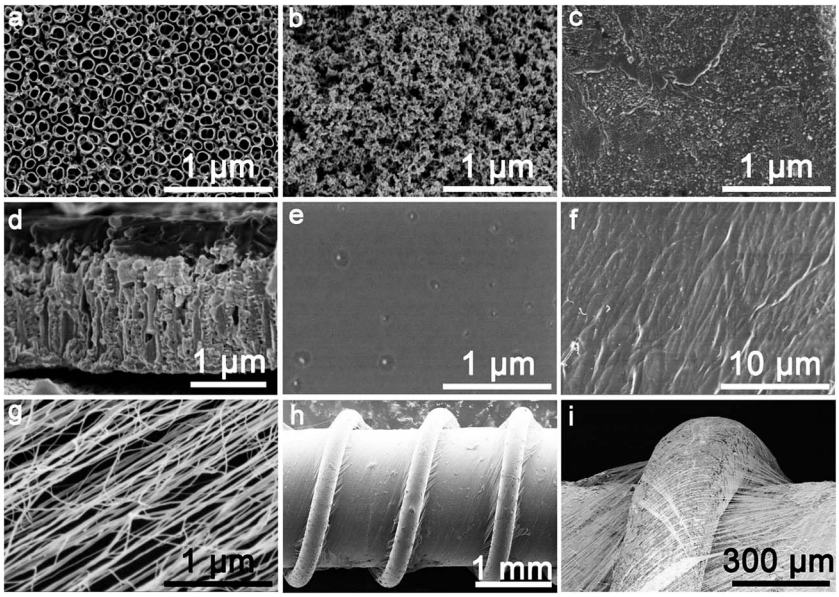


Fig. 3 SEM images of elastic PSC fibers. (a–c) Top view of aligned $TiO_2$ nanotubes, mesoporous $TiO_2$ nanoparticles and $CH_3NH_3PbI_{3-x}Cl_x$, respectively. (d) Cross-sectional image of the $TiO_2$ nanotube array coated with $CH_3NH_3PbI_{3-x}Cl_x$ and a hole transport layer. (e) Top view of the hole transport layer. (f and g) CNT sheet wrapped on the elastic fiber and modified Ti wire, respectively. (h) An elastic PSC fiber with a pitch distance of 1.25 mm. (i) High magnification of (h).

scanning electron microscope (SEM). Dense $TiO_2$ nanotubes were highly aligned and perpendicular to the outer surface of the Ti wire (Fig. S9†). Their diameters were centered at ~100 nm, and their lengths may be tuned by varying the growth time during electrochemical anodisation, *e.g.*, 0.4, 0.8, 1.3 and 1.7 μm at 10, 20, 30 and 40 min, respectively (Fig. S10†). $TiO_2$ nanoparticle layers with increasing thicknesses were produced by repeating the dip-coating process, *e.g.*, 0.9, 2.2, 3.6 and 5.8 μm for 5, 10, 15 and 20 times, respectively (Fig. S11 and S12†). Both $TiO_2$ nanotubes and nanoparticles offered high specific

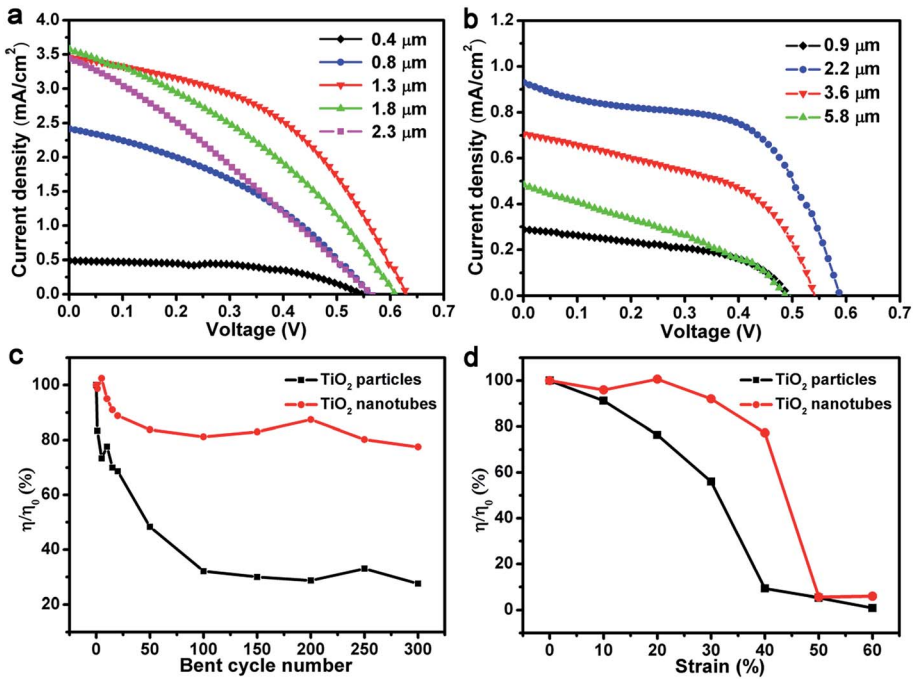


Fig. 4 *J*–*V* curves of elastic PSC fibers by varying the thickness of $TiO_2$ nanotubes (a) and mesoporous $TiO_2$ crystals (b). Dependence of energy conversion efficiency on the bent cycle number (c) and stretching strain (d). Here $\eta_0$ and $\eta$ correspond to the energy conversion efficiencies before and after bending or stretching, respectively.

surface areas for absorbing photoactive materials, and $CH_3NH_3PbI_{3-x}Cl_x$ can be further infiltrated into the bottom of $TiO_2$ materials, which was verified by SEM (Fig. 3c and d and S13†). Perovskite materials were well coated onto and had fully covered the spring-shaped electrode possibly because the aligned $TiO_2$ nanotubes were uniformly grown in both size and density (Fig. S14†), which was key to a high photovoltaic performance. Compared with a planar surface, it is generally much more difficult to produce continuous and uniform films on curved surfaces. Here the high coverage of the perovskite material on the fiber-shaped surface was attributed to the presence of 1,8-diiodooctane that chelated with $Pb^{2+}$ ions during the crystal growth, favoring the formation of high-quality thin perovskite films.[12,34] Similarly, a uniform hole transport layer had also been achieved on the perovskite film (Fig. 3d and e). The CNTs remained highly aligned after the CNT sheet was wrapped on the elastic rubber fiber (Fig. 3f). A single CNT sheet that was covered on the twisted modified Ti wire and elastic conductive fiber maintained the continuous structure and stably bundled the two fiber electrodes together (Fig. 3g–i). A CNT sheet was transparent with an optical transmittance of ~90% to ensure a high light absorption of photoactive materials (Fig. S6b and S15†).

Fig. 4a shows *J–V* curves of elastic PSC fibers with different lengths of $TiO_2$ nanotubes under the same conditions. The effective area was calculated according to Fig. S1† and is described in the Experimental section. The open-circuit voltages and short-circuit current densities were increased when the $TiO_2$ nanotubes were lengthened from 0.4 to 1.3 μm. As a result, the energy conversion efficiencies were enhanced from 0.16 to 1.01% (Fig. S16 and Table S1†). However, with the further increase in the length of $TiO_2$ nanotubes, the energy conversion efficiency was reduced to 0.78% and 0.56%. This phenomenon may be explained by the fact that too long $TiO_2$ nanotubes were relatively poorly infiltrated by perovskite precursors. The inadequate infiltration decreased the separation and collection efficiency of electrons and holes, resulting in low energy conversion efficiencies. Here an optimized length of 1.3 μm was mainly investigated below. Although the optimized thickness could be different for the different morphologies of nanoparticles and nanotubes, the tendency was the same. For the $TiO_2$ nanoparticles (Fig. 4b and S17†), the optimized thickness was obtained at 2.2 μm with the energy conversion efficiency of 0.31%. Generally, the PSC fibers derived from the aligned $TiO_2$ nanotubes exhibited higher energy conversion efficiencies than those based on $TiO_2$ nanoparticles as the $TiO_2$ nanoparticles could not be uniformly deposited on the surface of the spiral fiber. In addition, the structure of perpendicular nanotubes offered shorter pathways for charges to transport with higher speeds. The outermost CNT sheet was closely attached to the conductive elastic fiber to increase the hole collection. Without this CNT sheet, the energy conversion efficiency was decreased to 0.6% (Fig. S18†). Admittedly, the energy conversion efficiency of the fiber-shaped PSC was relatively low compared with their planar counterparts, which was owing to the difficulty in fabricating high-quality perovskite layers through dip-coating processes. To increase the energy conversion efficiencies, perovskite layers had also been fabricated by electrodeposition processes, and they could be enhanced to 5.01% after optimization (Fig. S19†). Generally, the energy conversion efficiencies ranged from 4.81% to 5.22%.

Fig. 4c and d further compare the dependence of energy conversion efficiency on the bent cycle number and strain in the elastic PSC fiber based on $TiO_2$ nanotubes and nanoparticles. The energy conversion efficiencies were maintained above 80% and 25% for $TiO_2$ nanotubes and nanoparticles under bending for 300 cycles, respectively; the energy conversion efficiencies were maintained above 90% and 50% for $TiO_2$ nanotubes and nanoparticles at a strain of 30%, respectively. Obviously, the use of perpendicularly grown $TiO_2$ nanotubes is more favorable for the development of flexible and elastic wearable devices. The elasticity was further investigated by stretching the PSC fiber at a strain of 30% for 250 cycles, and the energy conversion efficiency was maintained by 90% (Fig. 5a). These $TiO_2$ nanotubes could be more stably attached on the Ti wire for better bending and stretching performances. In addition, the spring-shaped electrode lessened the stress during stretching and bending, so the perovskite layer stayed unbroken (Fig. S20†).

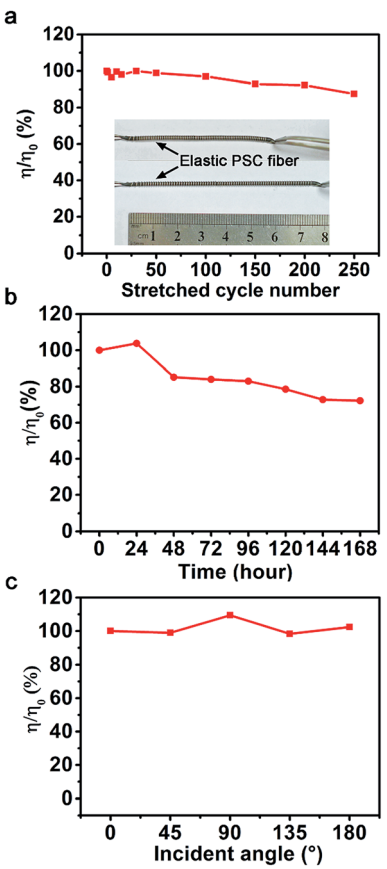


Fig. 5 (a) Dependence of energy conversion efficiency on the stretched cycle number. (Inset, photographs of an elastic PSC fiber before and after stretching, respectively). (b) Dependence of power conversion efficiency on time. (c) Dependence of energy conversion efficiency on the angle of incident light. Here $\eta_0$ and $\eta$ correspond to the energy conversion efficiencies at 0 and other angles, respectively.

 

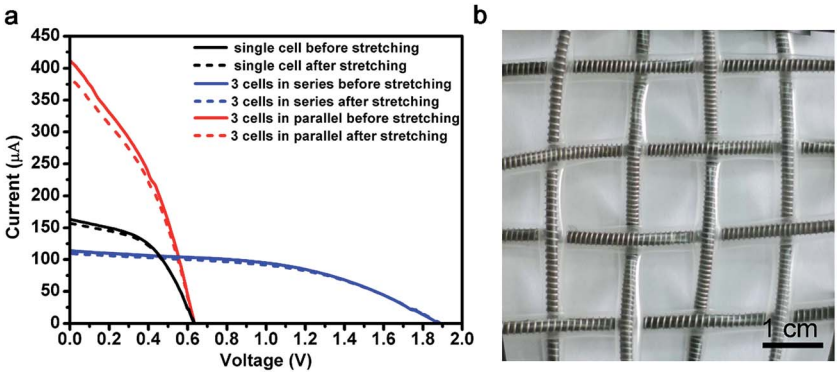


Fig. 6 (a) *J*–*V* curves of the resulting powering textile where three PSC fibers were connected in series or parallel before and after stretching. (b) Photograph of an elastic powering PSC textile.

The elastic PSC fiber was further studied for its stability by tracing the energy conversion efficiency during its use, and it retained ~80% after 168 h even without sealing (Fig. 5b). As expected, the energy conversion efficiencies remained almost unchanged when the PSC was irradiated in the angle range from 0 to 180° due to the unique one-dimensional shape (Fig. 5c). These elastic PSC fibers can be easily woven into textiles, and the PSC fibers can be connected in series or parallel to tune the output voltage or current, respectively. For instance, the output voltages were increased from 0.63 to 1.88 V when three PSC fibers were organized in series, while the output currents could be enhanced from 156 to 412 μA when they were connected in parallel (Fig. 6a). As expected, as individual PSC fibers were flexible and elastic, the resulting PSC textile was also flexible and elastic (Fig. 6b), which favored its application in flexible electronic devices.

## Conclusion

In summary, a new family of elastic perovskite solar cells has been developed with high photovoltaic performances by designing a spring-like Ti wire and CNT-based rubber fiber as two electrodes. The energy conversion efficiencies remained at 90% after stretching 250 times at a strain of 30%. Due to an all-solid-state structure and fiber shape, these PSC fibers can be further woven into electronic textiles for a large-scale application by the well-developed textile technology. This work also provides a general and effective strategy for the advancement of next-generation photovoltaic and other electronic devices.

## Acknowledgements

This work was supported by MOST (2011CB932503), NSFC (21225417, 51573027), STCSM (12nm0503200), the Fok Ying Tong Education Foundation, the Program for Special Appointments of Professors at Shanghai Institutions of Higher Learning, and the Program for Outstanding Young Scholars from the Organization Department of the CPC Central Committee.

## References

1 J. A. Rogers, T. Someya and Y. Huang, *Science*, 2010, **327**, 1603.
2 O. Schultz, S. W. Glunz and G. P. Willeke, *Prog. Photovoltaics*, 2004, **12**, 553.
3 Z. C. He, C. M. Zhong, S. J. Su, M. Xu, H. B. Wu and Y. Cao, *Nat. Photonics*, 2012, **6**, 591.
4 C. C. Chen, L. Dou, R. Zhu, C. H. Chung, T. B. Song, Y. B. Zheng, S. Hawks, G. Li, P. S. Weiss and Y. Yang, *ACS Nano*, 2012, **6**, 7185.
5 M. M. Lee, J. Teuscher, T. Miyasaka, T. N. Murakami and H. J. Snaith, *Science*, 2012, **338**, 643.
6 M. A. Green, A. H. Baillie and H. J. Snaith, *Nat. Photonics*, 2014, **8**, 506.
7 H. Zhou, Q. Chen, G. Li, S. Luo, T.-B. Song, H.-S. Duan, Z. Hong, J. You, Y. Liu and Y. Yang, *Science*, 2014, **345**, 542.
8 M. He, W. Han, J. Ge, Y. Yang, F. Qiu and Z. Lin, *Energy Environ. Sci.*, 2011, **4**, 2894.
9 M. He, D. Zheng, M. Wang, C. Lin and Z. Lin, *J. Mater. Chem. A*, 2014, **2**, 5994.
10 Z. Li, S. A. Kulkarni, P. P. Boix, E. Shi, A. Cao, K. Fu, S. K. Batabyal, J. Zhang, Q. Xiong, L. H. Wong, N. Mathews and S. G. Mhaisalkar, *ACS Nano*, 2014, **8**, 6797.
11 J. W. Lee, D. J. Seol, A. N. Cho and N. G. Park, *Adv. Mater.*, 2014, **26**, 4991.
12 P. W. Liang, C. Y. Liao, C. C. Chueh, F. Zuo, S. T. Williams, X. K. Xin, J. Lin and A. K. Jen, *Adv. Mater.*, 2014, **26**, 3748.
13 J. Ren, L. Li, C. Chen, X. Chen, Z. Cai, L. Qiu, Y. Wang, X. Zhu and H. Peng, *Adv. Mater.*, 2013, **25**, 1155.
14 T. Chen, L. Qiu, Z. Yang and H. Peng, *Chem. Soc. Rev.*, 2013, **42**, 5031.
15 C. Roldán-Carmona, O. Malinkiewicz, A. Soriano, G. Mínguez Espallargas, A. Garcia, P. Reinecke, T. Kroyer, M. I. Dar, M. K. Nazeeruddin and H. J. Bolink, *Energy Environ. Sci.*, 2014, **7**, 994.
16 P. Docampo, J. M. Ball, M. Darwich, G. E. Eperon and H. J. Snaith, *Nat. Commun.*, 2013, **4**, 2761.
17 D. Y. Liu and T. L. Kelly, *Nat. Photonics*, 2014, **8**, 133.

18 D. Zou, Z. Lv, X. Cai and S. Hou, *Nano Energy*, 2012, **1**, 273.
19 L. Qiu, J. Deng, X. Lu, Z. Yang and H. Peng, *Angew. Chem., Int. Ed.*, 2014, **53**, 10425–10428.
20 P. Roy, S. Berger and P. Schmuki, *Angew. Chem., Int. Ed.*, 2011, **50**, 2904.
21 J. M. Macak, H. Hildebrand, U. Marten-Jahns and P. Schmuki, *J. Electroanal. Chem.*, 2008, **621**, 254.
22 P. Liu, Q. Sun, F. Zhu, K. Liu, K. Jiang, L. Liu, Q. Li and S. Fan, *Nano lett.*, 2008, **8**, 647.
23 J. Wu, Y. Xiao, Q. Tang, G. Yue, J. Lin, M. Huang, Y. Huang, L. Fan, Z. Lan, S. Yin and T. Sato, *Adv. Mater.*, 2012, **24**, 1884.
24 S. D. Stranks, G. E. Eperon, G. Grancini, C. Menelaou, M. J. Alcocer, T. Leijtens, L. M. Herz, A. Petrozza and H. J. Snaith, *Science*, 2013, **342**, 341.
25 G. Xing, N. Mathews, S. Sun, S. S. Lim, Y. M. Lam, M. Gratzel, S. Mhaisalkar and T. C. Sum, *Science*, 2013, **342**, 344.
26 Y. Xiao, G. Han, Y. Li, M. Li, Y. Chang and J. Wu, *J. Mater. Chem. A*, 2014, **2**, 16531.
27 Y. Xiao, G. Han, Y. Li, M. Li and J. Wu, *J. Mater. Chem. A*, 2014, **2**, 16856.
28 L. Boilet, J. Cornard and C. Lapouge, *J. Phys. Chem. A*, 2005, **109**, 1952.
29 L. Qiu, X. Sun, Z. Yang, W. Guo and H. Peng, *Acta Chim. Sin.*, 2012, **70**, 1523.
30 S. Pan, Z. Yang, H. Li, L. Qiu, H. Sun and H. Peng, *J. Am. Chem. Soc.*, 2013, **135**, 10622.
31 J. Qiu, Y. Qiu, K. Yan, M. Zhong, C. Mu, H. Yan and S. Yang, *Nanoscale*, 2013, **5**, 3245.
32 H. S. Kim, J. W. Lee, N. Yantara, P. P. Boix, S. A. Kulkarni, S. Mhaisalkar, M. Gratzel and N. G. Park, *Nano Lett.*, 2013, **13**, 2412.
33 S. Dharani, H. K. Mulmudi, N. Yantara, P. T. Thu Trang, N. G. Park, M. Graetzel, S. Mhaisalkar, N. Mathews and P. P. Boix, *Nanoscale*, 2014, **6**, 1675.
34 G. E. Eperon, V. M. Burlakov, P. Docampo, A. Goriely and H. J. Snaith, *Adv. Funct. Mater.*, 2014, **24**, 151.